THE JOURNAL OF NAVIGATION (2021), **74**, 175–187.
doi:10.1017/S0373463320000466

Geolocal – A New System for Geo-Referencing: Analysis of Base Distribution

Eduardo P. Macho[1], Sergio V.D. Pamboukian[1] and Emília Correia[1,2]

[1](*CRAAM, Universidade Presbiteriana Mackenzie, São Paulo, Brazil*)
[2](*Instituto Nacional de Pesquisas Espaciais, São José dos Campos, Brazil*)
(E-mail: edu_point@hotmail.com)

Geolocal is a new navigation system conceived and patented in Brazil, whose purpose is to be independent of other global navigation satellite systems (GNSS). It has an 'inverted-GNSS' configuration with at least four bases on the ground at known geodesic position coordinates and a repeater in space. Simulations were performed to determine the precision of Geolocal using different quantities and distributions of bases. They showed that this precision is enhanced when the quantity of bases increases, as long as the elevation angles of the new bases included are higher than the average and when the bases are evenly distributed around the repeater, but mainly when the time delay at the repeater is known in advance and when the measurement errors that generate uncertainties are reduced. The position dilution of precision (PDOP) was also calculated, confirming that precision is enhanced by the quantity of bases and by their distribution.

KEYWORDS

1. Geolocal. 2. Inverted-GNSS. 3. PDOP.

Submitted: 4 March 2020. Accepted: 4 August 2020. First published online: 3 September 2020.

1. INTRODUCTION. Most countries depend on existing global navigation satellite systems (GNSS), mainly on the Global Positioning System (GPS) owned by the USA and operated by the United States Air Force. This is true not only for terrestrial navigation, but also for many critical and essential applications (Faria et al., 2016, 2018; Khan et al., 2020). Some of these applications are aerial and sea navigation, control of farming machinery, construction, mining, surveying, aerial photography, seaport automation, military and defence systems, economy, time accuracy, and ionospheric modelling (Islam and Kim, 2014; Li, Ge et al., 2015; Odolinski et al., 2020).

In order to be independent of GPS, several countries are developing their own systems. *Globalnaya Navigatsionnaya Sputnikovaya Sistema* (GLONASS), developed in Russia, can be combined with GPS (Maciuk, 2018; Gao et al., 2019), Galileo in Europe (Paziewski and Wielgosz, 2015) and BeiDou Navigation Satellite System (BDS) in China (Li, Zhang et al., 2015; Geng et al., 2019) using a global range GNSS, which can be integrated in

one multi-scale system for many applications. On the other hand, some countries are opting for a local configuration. Japan is using the Quasi Zenithal Satellite System (QZSS), a regional navigation satellite system compatible with GPS, for Asia-Pacific users (Zaminpardaz et al., 2018; Zhao et al., 2018). India has developed Navigation Using Indian Constellation (NavIC), designed to provide positioning services for the Indian mainland and up to 1,500 km around it as primary service area (Mandal et al., 2016; Santra et al., 2019). In Australia a private company, Locata, has created a technology based on a network of ground transmitters, working together with GPS or even independently, to cover a specific area with strong radio-positioning signals (Rizos and Yang, 2019).

There are also some alternative solutions without navigation satellites. The enhanced long-range navigation (eLoran) system is an evolution of the Loran system developed by the USA during the Second World War. It has the purpose of acting as a complement and backup to GNSS, especially in the maritime environment, with transmitters installed on ground towers near ports, providing a low-cost service and ensuring safety for sea navigation (Grunin et al., 2018). The Defence Science and Technology Laboratory (DSTL) in the United Kingdom has a research project on a system based on the concept of quantum position system (QPS) technology (Hong-Mei and Lu-Ping, 2016). It can improve positioning accuracy and clock synchronisation of submarine navigation, decreasing their positioning error, when afloat, from 1,000 m to 1 m per day (Krobka et al., 2016). The Doppler orbitography and radiopositioning integrated by satellite instrument (DORIS) from France is an uplink Doppler system that uses signals of two frequencies to track satellite positions and orbits. It consists of a worldwide network of transmission stations on the ground and receivers installed on low-orbit satellites (Kosek et al., 2020).

Following this trend, Brazil also has a work group developing a navigation system intended to be independent of current satellite systems without necessarily using navigation satellites for its purpose, named Geolocal. This new navigation system was conceived and patented by researchers of Mackenzie University (Kaufmann and Levit Kaufmann, 2012; Kaufmann et al., 2012, 2014; Pamboukian, 2012) and it is currently under the first phase of implementation.

The aim of this work is to perform an analysis of the best configuration of base stations in a chosen sector of a map. The analysis evaluates position errors considering bases randomly distributed in different locations to simulate a real scenario. The number of bases is gradually increased to identify the best number, in terms of cost-benefit, and the respective position error. The results are also compared with a position dilution of precision (PDOP) study.

2. DESCRIPTION OF GEOLOCAL.

The Brazilian system Geolocal has an 'inverted-GNSS' configuration and consists of at least four bases on the ground at known geodesic position coordinates. They can be distributed on the ground as bases *A*, *B*, *C* and *D* (Figure 1), synchronised among themselves, with a repeater *R* in space. The signal is transmitted from one of the ground bases, called the control base, e.g., base *A*, to the repeater *R* installed on a platform in space and retransmitted back to all the ground bases, including the control base.

Geolocal is a multidisciplinary project engaging several universities and institutes in Brazil. Its first implementation phase consists of defining the system topology, planning the field tests, developing and improving the processing algorithms, defining time reference

https://doi.org/10.1017/S0373463320000466 Published online by Cambridge University Press

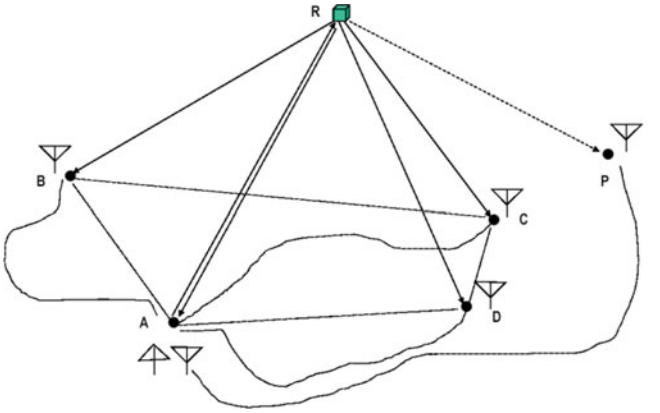

Figure 1. Simplified diagram of Geolocal, with four bases on the ground (*A*, *B*, *C*, *D*), with a repeater *R* in space and a target on the ground (*P*, to be used in a future phase).

and building prototypes of the stations. Once this phase is completed, the first application will involve the navigation of a flying platform carrying hardware intended to repeat the signal in space. Many platforms will benefit from this system: remotely piloted aircraft (RPA), popularly known as drones, scientific or weather balloons, commercial aircraft, and low-orbit satellites, including the 1210 CubeSats and 1317 Nanosats already launched (https://www.nanosats.eu/, April 2020). After the navigation of a repeater has become well established, a future phase of Geolocal will be the navigation of a target on the ground, e.g., target *P*, using a network of repeaters to find the target's position. The system will be independent of medium-orbit navigation satellites which are costly, are impacted by solar flares, and play a greater role in the increase of space junk.

The Geolocal system will consider the total propagation time of the signal transmitted by the ground bases and echoed on the repeater. From this total, time is subtracted for: the propagation time inside the instruments, cables and connectors at the transmission and at the final reception modules; the signal propagation delay through the medium causing path length variations; and the time of signal transit at the remote repeater. The result is multiplied by the speed of light to obtain the pseudo-distances from each ground base to the repeater. The repeater's position is then found by trilateration.

The signal delay time produced by the propagation inside the devices at ground bases can be obtained directly, and propagation delay through the medium between the base and repeater can be determined by a propagation model, which will depend on the altitude of the repeater. If the repeater is located in the troposphere or stratosphere (e.g., RPA, scientific balloon, commercial aircraft), it is necessary to consider the tropospheric refraction and signal delay caused by the gas composition of the neutral atmosphere. The main source of error in this region is the amount of water vapour in the tropospheric column (Duev et al., 2011; Facheris and Cuccoli, 2018). If the repeater is located at higher altitudes (e.g., CubeSat, Nanosat, and other satellites), where the signal propagates through the ionosphere, a propagation method that considers the delay caused by the refraction of the signal in the ionosphere should be applied. This can be done by determining the total electron content between the ground base and the repeater using the equations provided by Marković (2015). Scintillations also need to be considered for higher altitudes; they are rapid fluctuations in

https://doi.org/10.1017/S0373463320000466 Published online by Cambridge University Press

the amplitude and phase of radio signals produced by the ionospheric irregularities (Spogli et al., 2013; Correia et al., 2018). The time transit at the remote repeater can also be directly determined, before the platform (where the repeater is installed) is sent to space, or it can be calculated using the method demonstrated in the next section.

The radio frequencies that will be used in Geolocal have yet to be determined, as well as the clock between bases, which will be probably be a high precision atomic clock, such as cesium or rubidium.

3. METHOD. Software was developed to demonstrate the algorithm for Geolocal and to perform simulations using practical examples with a representation of ground-based reference bases. The simulation performed by Kaufmann et al. (2014) used, as ground bases, four cities in Brazil with known geodesic coordinates and synchronised clocks, and a receiver carried by an aircraft flying at an altitude of about 6 km over another city in the middle of the four bases. The results of this simulation demonstrated the method's functionality, with discrepancies in the repeater's position lower than 0·001 mm. In practice, the discrepancies are larger, due to: internal measurement errors at the transmitting and receiving bases, the path delay model chosen, and uncertainties of clock synchronisation. A new simulation was performed including these uncertainties and adopting a Gaussian distribution set in the root mean square range of ±0·5 ns. The errors obtained in this case were predominantly lower than 1 m in the repeater's position.

This work compares different distributions and different quantities of ground bases for one chosen repeater and verifies the error in the repeater's position for each case. Cases where the delay is known in advance in the repeater, where the delay is not known, and those obtained after minimising the uncertainties are included. A random distribution of fixed bases installed in several cities of Brazil covering an area of 240 × 140 km is considered. The locations of the fixed ground bases are shown in Figure 2.

The distances between the cities are of the order of 25 to 50 km, and these distances are suitable to find the position of a repeater placed at an altitude of the same magnitude, that is, in the Earth's stratosphere. One example of a platform compatible with this altitude is the scientific balloon, which can surpass altitudes of 50 km and fly for more than 40 days (Yamagami et al., 2004). For this present work, a scientific balloon is considered as a simulated platform where the repeater is meant to be installed, flying at an altitude of 30 km, over four different locations, also shown in Figure 2.

At tropospheric and stratospheric altitudes, the wave propagation bending caused by the Earth's curvature is insignificant compared with the delay due to the gas composition of the neutral atmosphere (Duev et al., 2011). The path delay model assumed in this work is the plane parallel model, described by Equation (1).

$$\Delta_{pd} = c\tau_{atm}/\sin H \tag{1}$$

where c is the speed of light, τ_{atm} is the atmosphere zenith delay, and H is the elevation angle of the platform. It is also necessary to consider the tropospheric delay, which consists of a 'dry' or hydrostatic part that is relatively stable, and a 'wet' part that depends on the water vapour content where the bases are installed (Honma et al., 2008). The corrections along the path of the signals can be derived from the zenith delay using mapping functions (Niell, 1996).

https://doi.org/10.1017/S0373463320000466 Published online by Cambridge University Press

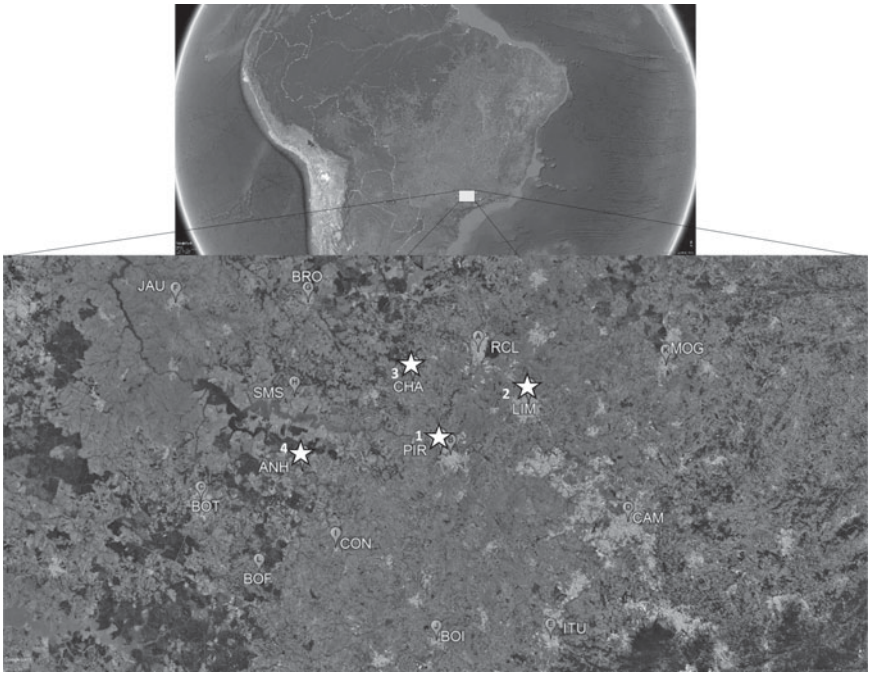

Figure 2. Satellite image of an area in Brazil, with 12 ground bases (*A* to *L*), and four repeaters positioned in different locations (each repeater represented by a star) (adapted from Google Earth).

The first step of this method is to transform the positioning system from LLA (latitude, longitude, altitude) to ECEF (Earth centred, Earth fixed) using datum WGS84 for the reference ellipsoid. In the LLA system, the latitude varies between 0° and 90° from the Equator to north (positive) or south (negative) and the longitude varies between 0° and 180° from the Greenwich Meridian to east (positive) or west (negative). In the ECEF system, the origin is located in the centre of the Earth's mass, the x, y and z axes are fixed and rotate with the planet: z pointing to the North Pole and x pointing to the intersection between the Greenwich Meridian with the Equator line (μ-BLOX, 1999). To do this ellipsoidally to Cartesian transformation, Equations (2)–(4) are used, where φ is the latitude, λ is the longitude, N is the prime radius of curvature of the geoid, h is the height, a is the major semi-axis, and b is the minor semi-axis of the Earth's ellipsoid.

$$x = (N + h)\cos\varphi\cos\lambda \tag{2}$$

$$y = (N + h)\cos\varphi\sin\lambda \tag{3}$$

$$z = \left(\frac{b^2}{a^2}N + h\right)\sin\varphi \tag{4}$$

Equation (5) is used to calculate the spatial distances between the bases and each location of the repeater, where n represents each base.

$$dn = \sqrt{(dx)^2 + (dy)^2 + (dz)^2} \tag{5}$$

https://doi.org/10.1017/S0373463320000466 Published online by Cambridge University Press

For all the simulations, a fixed value was adopted for the well-measured delays due to the signal passing to electronics, cables and connectors on the transmitting control base, e.g., base A of Figure 1 (δ_{At}), and reception bases ($\delta_{Ar}, \delta_{Br}, \delta_{Cr}, \ldots, \delta_{nr}$) as 0·0001 ms. Adopting c = 299, 792, 458 m/s, the distance from the control base to the repeater (d_A) is given by Equation (6), and the distance from the other bases to the repeater (d_n) is given by Equation (7).

$$d_A\left(\delta_R, \Delta_{pd(\mathrm{AR})}\right) = \left(\Delta t_A - \delta_{At} - \delta_{Ar} - \delta_R\right)\left(\frac{c}{2}\right) - \Delta_{pd(\mathrm{AR})} \tag{6}$$

where δ_R is the time delay of the signal at the repeater; $\Delta_{pd(AR)}$ is the path delay through the medium between the control base and the repeater; and Δt_A is the measured propagation time of the signal from the control base to the repeater and back to the control base.

$$d_n\left(\delta_R, \Delta_{pd(AR),}\Delta_{pd(nR)}\right) = \left(\Delta t_n - \delta_{At} - \delta_{nr} - \delta_R\right)(c) - d_A\left(\delta_R\right) - \Delta_{pd(AR)} - \Delta_{pd(nR)} \tag{7}$$

where $\Delta_{pd(nR)}$ is the path delay through the medium between each base (except control base) to the repeater; and Δt_n is the measured propagation time of the signal from each base to the repeater and back to each base.

If there is access to the platform where the repeater is installed, δ_R can be directly measured, it being necessary only to calculate Δ_{pd} to find the position of the repeater. In case we do not have access to it, which will be the case when the repeater is installed in a third-party platform, it is necessary to use the iterative method below to find both δ_R and Δ_{pd}.

The iterative method consists in calculating the repeater's position using all possible sets of three bases, always including the control base. For the case of four bases, the sets would be *A-B-C*, *A-B-D* and *A-C-D*. These sets are used to find three different positions for the repeater (*Ra*, *Rb* and *Rc*). For each set, an initial value is adopted for Δ_{pd} and δ_R and setting a lower and upper range for δ_R variation. For this simulation, an initial value was adopted for Δ_{pd} as zero and for δ_R as 100 ns, ranging from 0 ns to 1000 ns.

In the first iteration of the first set of bases (*A-B-C*), the elevation angles of the repeater with respect to each base are found using the adopted initial values and, by using Equation (1), Δ_{pd} can also be found. The next step is to use the new value of Δ_{pd}, which is no longer zero, to recalculate the position *Ra* of the repeater. This reiterative process is done until the values converge.

The same process is repeated with the other sets to find *Rb* and *Rc*. The error in the repeater's position is calculated by: $\|Ra - Rb\| + \|Rb - Rc\| + \|Rc - Ra\|$. Because δ_R was adopted within an interval, the calculation is repeated for different values of δ_R, until the error becomes minimised. The correct values of all Δ_{pd} and δ_R are found at the end of the minimisation process. These values, together with the propagation delays at transmission and receiver bases (that can be measured directly) are subtracted from the total propagation time, and the result, multiplied by the speed of light, gives the pseudo-distance from each base to the repeater.

The simulations performed in this work start with four ground bases, and this quantity is increased gradually to verify what is the best cost-benefit scenario according to the number of bases, from four to 12 bases, so several quantities of bases are available for analysis.

4. RESULTS AND DISCUSSION. The four different simulation conditions of Geolocal, representing four possible uncertainties, are shown in Table 1.

https://doi.org/10.1017/S0373463320000466 Published online by Cambridge University Press

Table 1. Geolocal simulation conditions.

Condition	σ	δ_R
a	3·3 ns	to be calculated
b	3·3 ns	200 ns
c	0·5 ns	to be calculated
d	0·5 ns	200 ns

- Condition (a) considers a higher level of uncertainty when taking into account errors due to delay measurements at transmitting and receiving bases, to the chosen path delay model, and mainly to clock synchronisation between ground bases. It has a Gaussian distribution of measurement errors with a standard deviation (σ) of 3·3 ns, and the time delay at the repeater is unknown.
- Condition (b) also has $\sigma = 3 \cdot 3$ ns, but the time delay at the repeater is known in advance ($\delta_R = 200$ ns), so it does not need to be calculated.
- Condition (c) has $\sigma = 0{\cdot}5$ ns, which is a lower level of uncertainty with unknown time delay at the repeater.
- Condition (d) has $\sigma = 0 \cdot 5$ ns with a known time delay at the repeater ($\delta_R = 200$ ns).

These σ values were chosen to verify if a substantial reduction of uncertainty would be able to improve the position accuracy.

For each of the four conditions, 1,000 simulations were performed, considering the distinct locations of the repeater – *R1*, *R2*, *R3* and *R4* (shown in Figure 2 as PIR, LIM, CHA and ANH, respectively) – starting with bases *A*, *B*, *C* and *D* (shown in Figure 2 as RCL, PIR, BOT and CAM). They form a triangle on the map with base *B* in the middle and the location *R1* at the zenith of base *B* (altitude above sea level of base *B* is 534 m and *R1* 30 km). Configurations with more than four bases were also considered, by adding one by one, from *E* to *L*, and performing the simulations for each case.

(a) The results of condition (a) are shown in Figure 3, which represents the average of error in the repeater's position of 1,000 simulations for each repeater's location, indicating how the error evolves as each new ground base is added into the system. Figure 3 shows that if four bases are used the error in the repeater's position is lower when the elevation angles of the repeater, as seen by the bases, are higher on average. In most of the simulations for location *R*1 the errors are lower than 6 m, with an average of 2·32 m, and its elevation angles from bases *A*, *B*, *C* and *D* are primarily higher than the other locations: 38·90°, 83·36°, 19·63° and 23·69°, respectively (average: 41·39°). For locations *R2* and *R3* most of the simulations have errors lower than 8 m, with averages of 3·20 and 3·00 m, respectively, and elevations of 50·52°, 43·48°, 14·29° and 29·64° for *R2* (average: 34·48°) and 50·74°, 47·19°, 19·69° and 18·86° for *R3* (average: 34·12°). Location *R4* has simulations with higher errors, up to 16 m (average: 5·60 m), with the lowest average of elevation angles, and therefore it is more influenced by the path delay through the atmosphere. Elevations of *R4* are 22·49°, 30·57°, 39·36° and 14·88° (average: 26·82°).

As the number of ground bases increases, the errors in the repeater's position decrease slowly for locations *R1*, *R2* and *R3*, and quickly for location *R4* until the number of nine bases (from *A* to *I*) is achieved. The changes in the errors depend on whether the new bases added into the simulations increase or decrease the average of the elevation angles, and also on their locations relative to the locations of the previous bases. The simulations show that

https://doi.org/10.1017/S0373463320000466 Published online by Cambridge University Press

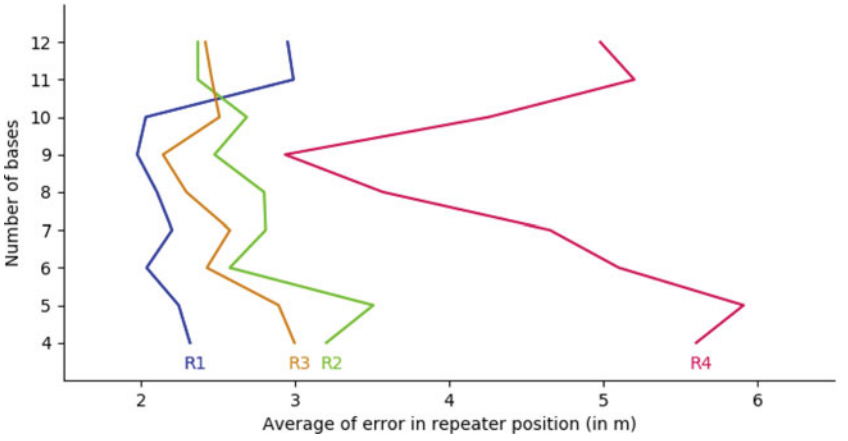

Figure 3. Average of error in the repeater's position using $\sigma = 3 \cdot 3$ ns, for 1,000 simulations, including the calculation of time delay at the repeater, for different quantities of bases and location of repeater.

when the distribution of the bases including a newly added base becomes more evenly scattered, the error in the repeater's position tends to decrease. When the base added is placed near another base, or aligned to it in relation to the repeater, the error tends to increase. Location *R4* has the most noticeable variation, with errors down to an average of 2·94 m with nine bases, and increasing, when base *J* is added to the simulation, to an average of 4·26 m, and, with the addition of base *K*, to an average of 5·20 m. This happens due to the elevation angles of *R4*, which are 22·17° and 13·04° from bases *J* and *K* respectively, much lower than the average elevation angle of bases *A* to *I*, which is 30·06°, and also because base *J* is somewhat aligned with base *I* and *R4*, and base *K* with base *B* and *R4*. When base *L* (elevation angle of R4: 38·32°) is included into the simulation, the average of errors decreases again to 4·98 m, because it improves the distribution of bases and the elevation angle is higher than the average. In a real scenario, the errors could be minimised by setting a cutoff angle, e.g., of 15°, into the system.

(b) The results of condition (b) are shown in Figure 4. It can be noted that the errors in the repeater's position decrease slowly for locations *R1*, *R2* and *R3* from four to 12 bases (up to base *L*), and quickly for location *R4* from four to nine bases (up to base *I*), and they increase for *R4* after the addition of bases *J* and *K*, and decrease after the addition of base *L*. The errors in the repeater's position of (b) are lower than (a): in (a), all errors are lower than 10 m for *R1*, *R2* and *R3*, and 16 m for *R4*, and in (b), all errors are lower than 5 m for *R1*, *R2* and *R3*, and 10 m for *R4*. The averages of errors of the locations *R1*, *R2*, *R3* and *R4* in (b), considering four bases as an example, are respectively 1·56, 1·64, 1·58, and 2·82 m; lower than (a) with 2·32, 3·20, 3·00 and 5·60 m. These results indicate that when we know the time delay at the repeater in advance, the errors decrease to nearly half.

(c) The results of condition (c) are shown in Figure 5. The pattern of (c) is similar to (a) for *R1*, *R2*, *R3* and *R4*, but the errors in the repeater's position in (c) are much lower, with all errors lower than 2 m for *R1*, *R2* and *R3* and lower than 3 m for *R4*. The averages are 0·35, 0·49, 0·45, and 0·88 m, around 15% of (a) values. That means that the reduction of around 85% of σ (from 3·3 to 0·5 ns) of the distribution of errors of measurements included in the simulation causes a reduction in errors in the repeater's position of the same amount.

https://doi.org/10.1017/S0373463320000466 Published online by Cambridge University Press

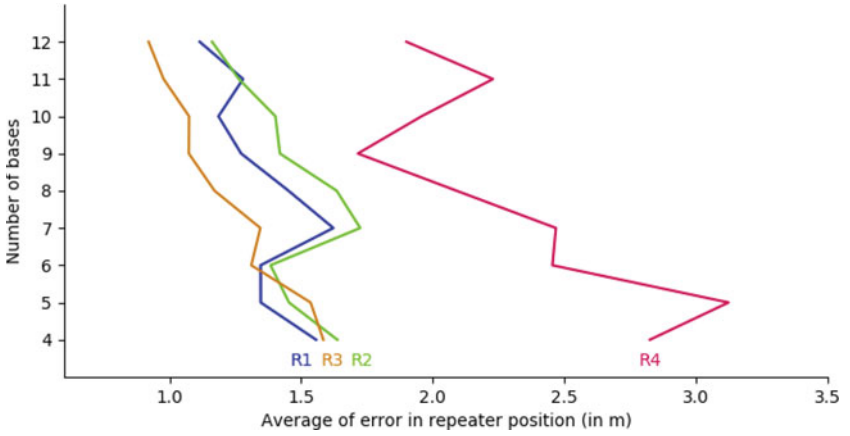

Figure 4. Same scenario as Figure 3, with a given δ_R (200 ns).

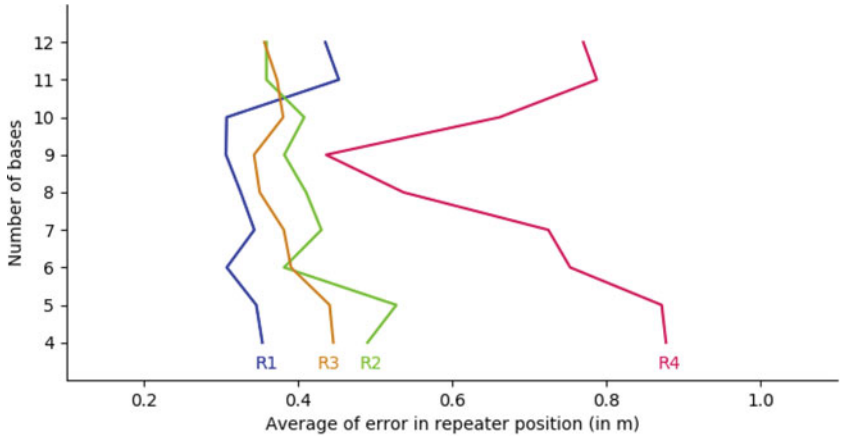

Figure 5. Same scenario as Figure 3, with σ = 0·5 ns.

(d) The results of condition (d) are shown in Figure 6. The pattern of (d) is similar to (b) for *R1*, *R2*, *R3* and *R4*, but the errors in the repeater's position in (d) are much lower. All errors are lower than 0·8 m for *R1*, *R2* and *R3*, and lower than 1·7 m for *R4*. The averages are 0·23, 0·24, 0·25, and 0·43 m, around 15% of (b) values, and nearly half of (c). These results confirm that the reduction in the errors in the repeater's position is proportional to the reduction in σ of the distribution of measurement errors included in the simulation, and also that knowing the time delay at the repeater in advance, these errors decrease to nearly half.

5. COMPARING THE RESULTS WITH PDOP. In this section, the error in the repeater's position is compared with the PDOP for each quantity and distribution of bases. PDOP is a very efficient tool to evaluate the geometry of a navigation system, and it is possible to use PDOP to quantify the precision of a repeater's position in space according to the distribution of fixed bases on Earth. It is a coefficient that, when multiplied by the standard

https://doi.org/10.1017/S0373463320000466 Published online by Cambridge University Press

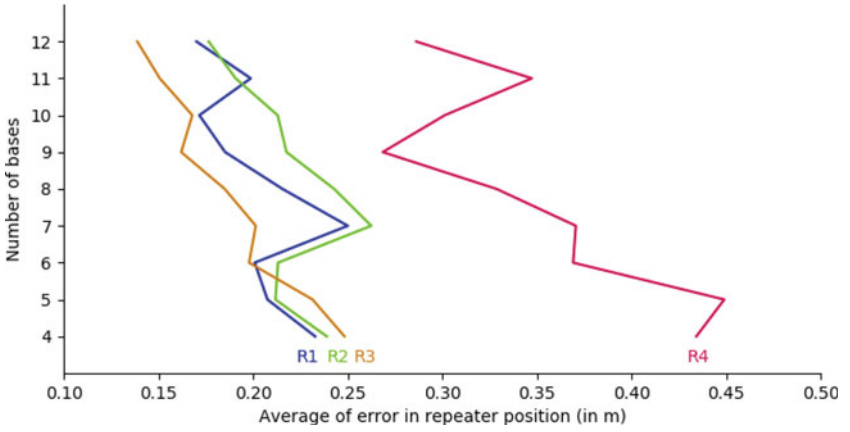

Figure 6. Same scenario as Figure 3, with $\sigma = 0{\cdot}5$ ns and $\delta_R = 200$ ns.

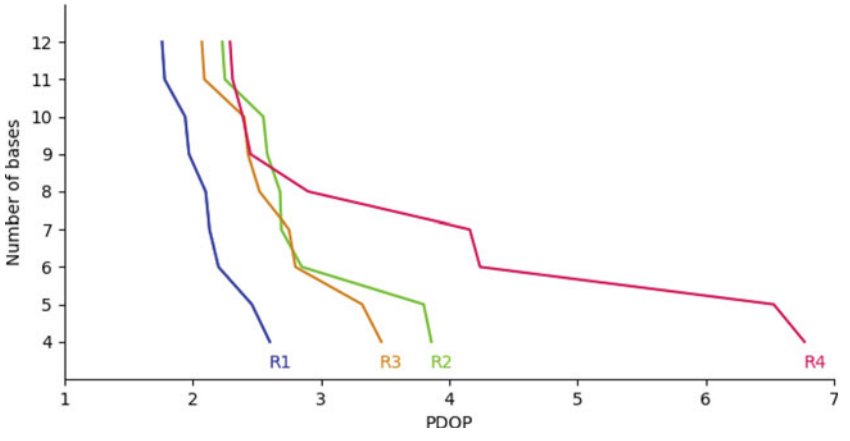

Figure 7. PDOP values for different quantities of bases and location of repeater.

deviation of error of the pseudo-distance measurements between a repeater and the bases seen by the repeater, results in the standard deviation of the error in the repeater's position. The ideal value is one, but values lower than four are acceptable for most applications.

This study uses the well-known PDOP equations given by Phillips (1984). For this calculation, the same sequence of bases is chosen as in the previous simulations, starting with four bases, *A*, *B*, *C* and *D* of Figure 2, and increasing one by one, from *E* to *L*, for each of the four locations of the repeater installed in a scientific balloon, *R1* to *R4*, flying at an altitude of 30 km. The results shown in Figure 7 are the PDOP values for each quantity of bases for different locations of the repeater.

The location *R1* has the best precision (lower PDOP values), which is equivalent to the error in the repeater's position with lower quantities of bases (Figures 3–6). However, in contrast with the errors, which increase when the bases added generate lower elevation angles, PDOP always decreases as the quantity of bases increases. The location *R1* also has the advantage of being near the zenith of a base, helping with the reduction of PDOP,

https://doi.org/10.1017/S0373463320000466 Published online by Cambridge University Press

especially when the number of bases is low, in this case, four or five bases. For a larger quantity of bases, placing the repeater near the zenith of a base does not improve the accuracy substantially. This is crucial, because it is unlikely that the repeater would be at the zenith of a base in a real situation.

Following *R1*, there are the locations *R2* and *R3*. With a lower quantity of bases, these have lower precision than *R1*, but higher than *R4*, due to the geometry and distribution of the bases. The same happens with the errors. For a higher quantity of bases, the PDOP values converge to values between two and three.

The worst case, for a lower quantity of bases, is found for location *R4*, which has the highest PDOP values, because the distribution of bases from *R4*'s point of view is less favourable. This is also equivalent to errors in the repeater's position. The PDOP also converge to values between two and three when adding bases.

The acceptable condition of PDOP lower than four is found with eight or more bases. To increase the precision even more, and to include overdetermination, it is recommended either to use more bases in a real situation, e.g., establishing a minimum quantity of 10 bases, or to make sure the bases are evenly distributed.

6. CONCLUSION. This paper has presented how the distribution of different numbers of ground base stations across a chosen area affects the precision of Geolocal, a Brazilian navigation system. Simulations of Geolocal were used to determine the position of a repeater installed in a scientific balloon flying at 30 km of altitude, quantified by the deviation in the repeater's position, in meters, from its actual position. The study also used, as a basis of comparison, the PDOP coefficient.

The precision of Geolocal is improved by the increase in the number of bases used in the system, as long as the elevation angles of the repeater seen by the new bases are higher than the average, and also improved by how the bases are distributed through the area, in relation to the repeater. The precision is higher when the ground bases are more homogenously distributed around the repeater, and lower when the bases are concentrated at certain regions. Although PDOP is not influenced by elevation angles, as it is not affected by the atmospheric content, it is highly influenced by the number of bases and, mainly, by their distribution. For a low quantity of bases, such as four or five bases, PDOP decreases when the repeater is located at the zenith of a central base, but when more bases are included, this characteristic becomes less important.

The greatest improvement in the precision, however, is achieved in two ways. The first is to measure the time delay of the signal at the repeater prior to sending the repeater into space (conditions b and d). In this case, the errors in the repeater's position decrease to nearly half. The second is to reduce the uncertainties caused by measurement errors at the transmitting and receiving bases, due to the path delay model chosen, and mainly to clock delay uncertainties (conditions c and d). This reduction can be done by using precise atomic clocks, such as cesium or rubidium. In this case, the decrease of error in the repeater's position is proportional to the decrease in the standard deviation of measurement errors distribution included in the simulations. With these improvements, the best cost-benefit scenario can be achieved by using a lower quantity of bases, as long as the elevation angles are not too low, so the use of a cutoff angle, e.g., 15°, is highly recommended.

ACKNOWLEDGEMENTS

The authors acknowledge Coordenação de Aperfeiçoamento de Pessoal de Nível Superior Brasil (CAPES) for the financial support in providing scholarship funding through Financial Code 001 and Fundo Mackenzie de Pesquisa (MACKPESQUISA) for financial support. EC thanks the National Council for Scientific and Technological Development (CNPq) (processes: 556872/2009-6, 406690/2013-8 and 306142/2013-9) and São Paulo Research Foundation (FAPESP) (process: 2019/05455-2) for individual research support.

REFERENCES

μ−BLOX (1999). Datum Transformations of GPS Positions. https://microem.ru/files/2012/08/GPS.G1-X-00006.pdf. Accessed 27 February 2020.

Correia, E., Muella, M. T. A. H., Alfonsi, L., Prol, F. S. and Camargo, P. O. (2018). GPS scintillations and total electron content climatology in the southern American sector. In: Ugur Sanli, D. (ed.). *Positioning Accuracy of GNSS Methods*. IntechOpen, London, 47–70. doi:10.5772/intechopen.79218.

Duev, D. A., Pogrebenko, S. V. and Calvés, G. M. (2011). A tropospheric signal delay model for radio astronomical observations. *Astronomy Reports*, **55**(11), 1008–1015.

Facheris, L. and Cuccoli, F. (2018). Global ECMWF analysis data for estimating the water vapor content between two LEO satellites through NDSA measurements. *IEEE Transactions on Geoscience and Remote Sensing*, **56**(3), 1546–1554.

Faria, L. A., Silvestre, C. A. M. and Correia, M. A. F. (2016). GPS-dependent systems: vulnerabilities to electromagnetic attacks. *Journal of Aerospace Technology and Management*, **8**(4), 423–430.

Faria, L. A., Silvestre, C. A. M., Correia, M. A. F. and Roso, N. A. (2018). Susceptibility of GPS-dependent complex systems to spoofing. *Journal of Aerospace Technology and Management*, **10**, e0218.

Gao, W., Pan, S., Gao, C., Wang, Q. and Shang, R. (2019). Tightly combined GPS and GLONASS for RTK positioning with consideration of differential inter-system phase bias. *Measurement Science and Technology*, **30**(5), 054001.

Geng, J., Li, X., Zhao, Q. and Li, G. (2019). Inter-system PPP ambiguity resolution between GPS and BeiDou for rapid initialization. *Journal of Geodesy*, **93**, 383–398.

Grunin, A., Kalinov, G., Bolokhovtsev, A. and Sai, S. (2018). Method to improve accuracy of positioning object by eLoran system with applying standard Kalman filter. *Journal of Physics: Conference Series*, 1015, 032050.

Hong-Mei, H. and Lu-Ping, X. (2016). Design and analysis of the secure scheme for quantum positioning based on photon pair. *International Journal of Technology and Human Interaction*, **12**(2), 22–35.

Honma, M., Tamura, Y. and Reid, M. J. (2008). Tropospheric delay calibrations for VERA. *Publications of the Astronomical Society of Japan*, **60**, 951–960.

Islam, M. R. and Kim, J. M. (2014). An effective approach to improving low-cost GPS-positioning accuracy in real-time navigation. *The Scientific World Journal*. **4**, 1–8.

Kaufmann, P. and Levit Kaufmann, P. (2012). Process and System to Determine Temporal Changes in Retransmission and Propagation of Signals Used to Measure Distances, Synchronize Actuators and Georeference Applications. Patent of Invention PI03003968-4, filed in Brazil on 19 March 2012, International PCT, application filed on 17 April 2012.

Kaufmann, P., Levit Kaufmann, P., Pamboukian, S. V. D. and Vilhena de Moraes, R. (2012). Signal transceiver transit times and propagation delay corrections for ranging and georeferencing applications. *Mathematical Problems in Engineering*, 2012, **89**, 1–12.

Kaufmann, P., Levit Kaufmann, P., Pamboukian, S. V. D. and Vilhena de Moraes, R. (2014). A new independent GPS-free system for geo-referencing from space. *Scientific Research*, **5**, 37–45.

Khan, A. M., Iqbal, N., Khan, A. A., Khan, M. F. and Ahmed, A. (2020). Detection of intermediate spoofing attack on global navigation satellite system receiver through slope based metrics. *The Journal of Navigation*, **73**(5), 1052–1068.

Kosek, W., Popinski, W., Wnek, A., Sosnika, K. and Zbylut-Gorska, M. (2020). Analysis of systematic errors in geocenter coordinates determined from GNSS, SLR, DORIS, and GRACE. *Pure and Applied Geophysics*, **177**, 867–888.

Krobka, N. I., Tribulev, N. V. and Bidenko, A. I. (2016). The Projects on Application of Atom Interferometer in Space and Sea: Current State. *23rd Saint Petersburg International Conference on Integrated Navigation Systems*. May 2016.

Li, X., Ge, M., Dai, X., Ren, X., Fritsche, M., Wickert, J. and Schuh, H. (2015). Accuracy and reliability of multi-GNSS real-time precise positioning: GPS, GLONASS, BeiDou, and Galileo. *Journal of Geodesy*, **89**(6), 607–635.

Li, X., Zhang, X., Ren, X., Fritsche, M., Wickert, J. and Schuh, H. (2015). Precise positioning with current multi-constellation global navigation satellite systems: GPS, GLONASS, Galileo and BeiDou. *Nature Scientific Reports*, **5**, 8328.

Maciuk, K. (2018). GPS-only, GLONASS-only and combined GPS + GLONASS absolute positioning under different sky view conditions. *Tehniéki vjesnik*, **25**(3), 933–939.

Mandal, S., Samanta, K. and Bose, A. (2016). IRNSS and Possible Benefits in Hybrid Operation with GPS. *Proc. National Conference on Materials, Devices and Circuits for Communication Technology, Burdwan, India*, 19–20 February, 72–75.

Marković, M. (2015). Determination of total electron content in the ionosphere using GPS technology. *Geonauka*, **02**, 1–9.

Niell, A. E. (1996). Global mapping functions for the atmosphere delay at radio wavelengths. *Journal of Geophysical Research*, **101**(B2), 3227–3246.

Odolinski, R., Teunissen, P. J. G. and Zhang, B. (2020). Multi-GNSS processing, positioning and applications. *Journal of Spatial Science*, **65**(1), 3–5.

Pamboukian, S. V. D. (2012). Novo processo de georeferenciamento: determinação de posição de transponder remoto e aplicações no posicionamento de alvos e disseminação de tempos. *Software Registered in Brazil*. Protocol 02012-0032225.

Paziewski, J. and Wielgosz, P. (2015). Accounting for Galileo-GPS inter-system biases in precise satellite positioning. *Journal of Geodesy*, **89**, 81–93.

Phillips, A. (1984). Geometrical determination of PDOP. *Journal of the Institute of Navigation*, **31**(4), 329–337.

Rizos, C. and Yang, L. (2019). Background and recent advances in the Locata terrestrial positioning and timing technology. *Sensors (Basel)*, **19**(8), 1821.

Santra, A., Mahato, S., Mandal, S., Dan, S., Verma, P., Banerjee, P. and Bose, A. (2019). Augmentation of GNSS utility by IRNSS/NavIC constellation over the Indian region. *Advances in Space Research*, **63**, 2995–3008.

Spogli, L., Alfonsi, L., Cilliers, P. J., Correia, E., De Franceschi, G. D., Mitchell, C. N., Romano, V., Kinrade, J. and Cabrera, M. A. (2013). GPS scintillations and total electron content climatology in the southern low, middle and high latitude regions. *Annals of Geophysics*, **56**(2), R0220.

Yamagami, T., Saito, Y., Matsuzaka, Y., Namiki, M., Toriumi, M., Yokota, R., Hirosawa, H. and Matsushima, K. (2004). Development of the highest altitude balloon. *Advances in Space Research*, **33**, 1653–1659.

Zaminpardaz, S., Wang, K. and Teunissen, P. J. G. (2018). Australia-first high-precision positioning results with new Japanese QZSS regional satellite system. *GPS Solutions*, **22**, 101.

Zhao, Q., Chen, G., Guo, J., Liu, J. and Liu, X. (2018). An a priori solar radiation pressure model for the QZSS Michibiki satellite. *Journal of Geodesy*, **92**(2), 109–121.